Green Chemistry

PAPER

View Article Online
View Journal | View Issue

Cite this: *Green Chem.*, 2020, **22**, 7398

p-Xylene from 2,5-dimethylfuran and acrylic acid using zeolite in a continuous flow system†

Jose Alirio Mendoza Mesa, [a,b] Francesco Brandi, [a] Irina Shekova, [a] Markus Antonietti [a] and Majd Al-Naji *[a]

Received 4th May 2020,
Accepted 3rd September 2020

DOI: 10.1039/d0gc01517b

rsc.li/greenchem

The continuous flow synthesis of *p*-xylene (*p*XL) *via* Diels–Alder cycloaddition of lignocellulosic biomass-derivable 2,5-dimethylfuran (DMF) and acrylic acid (AA) was performed over different type of zeolites, *i.e.* Beta, ZSM-5 and Y. Among the tested zeolites, Beta zeolite showed an optimum catalytic performance in *p*XL synthesis from DMF and AA. In this context, Beta zeolite with a Si/Al molar ratio of 150 which is abbreviated as Beta(150), resulted in complete DMF conversion with a *p*XL yield of 83% and by-product 2,5-dimethylbenzoic acid (DMBA) with a yield of 17%, at 473 K in 10.1 min residence time (τ), with excess AA (0.7 M). This high catalytic activity is attributed to the high specific surface area of 1180 $m^2\ g^{-1}$ with a three-dimensional porous architecture with a pore diameter of 6.6 × 6.7 Å and an acid site density above 40 μmol g^{-1}. The utilized Beta(150) showed a very stable performance up to 10 h time on stream with minor deactivation after 8 h of TOS, while the *p*XL yield remained above 70%. The original catalytic performance of Beta(150) in the conversion of DMF to *p*XL was restored by applying a regeneration step for the spent catalyst, which is simple in continuous flow reactors. Finally, this sustainable continuous flow process enables an efficient and selective *p*XL production from DMF and AA as a dienophile at lower reaction temperature (473 K) and shorter residence time (τ = 10.1 min) in comparison to a batch fashion.

Introduction

From the beginning of industrialization, our society has developed a heavy dependence on coal and fossil oils as a source of energy and chemicals.[1–7] This has led to the well-known environmental side effects that we are facing today. In order to decrease the dependency on fossil resources, alternative methodologies to produce fine chemicals from renewable resources, *e.g.* lignocellulosic biomass, with low environmental impact are greatly needed.[1–11] In this regard, a large number of publications have described the utilization of waste lignocellulosic biomass-derived compounds for the synthesis of fine chemicals, *e.g.* sugars, 5-hydroxymethylfurfural (HMF), 2,5-dimethylfuran (DMF) and levulinic acid (LA).[12–19] Among these is DMF which is produced simply by the catalytic hydrogenation of HMF.[1,15] DMF is not only a high-quality biofuel, but can be used as a precursor for the synthesis of a high value platform chemical, *e.g.* *p*-xylene (*p*XL).[1,15,20–24]

In 2015, around 37 million metric tons of *p*XL were consumed mostly for the production of poly(ethylene terephthalate) (PET) and polyester fiber.[23–26] There are reported studies on the synthesis of *p*XL from biomass-derived DMF, which include a Diels–Alder cycloaddition of ethylene to form the intermediate 1,4 dimethyl-7-oxabicyclo[2.2.1]hept-2-ene, followed by a dehydration step to *p*XL using different types of zeolites as catalysts.[23–29] Usually, for this reaction batch systems are used, combined with high reaction temperatures (523 K–623 K), high ethylene pressures (5.0 MPa–7.0 MPa) and long reaction times (24 h–48 h).[30] All these are less appealing in terms of green chemistry. Williams *et al.*[30] have reported a 75% yield of *p*XL as a result of cycloaddition of ethylene to DMF using H–Y zeolite at 573 K. Moreover, diverse side products from a competitive reaction on H–Y zeolite were found under the reported reaction conditions, *i.e.* 2,5-hexanedione, *p*XL alkylation products and polycondensates of 2,5-hexanedione.[30,31] H-Beta zeolite with a Si/Al ratio of 12.5 showed higher selectivity toward *p*XL compared to H-FAU and H-ZSM-5 at 523 K and 6.2 MPa of ethylene.[30,32] This high performance of H-Beta is attributed to its resistance to deactivation and its ability to selectively catalyze the dehydration of Diels–Alder cycloaddition intermediates to *p*XL.[30,32,33] Phosphorus modification of Beta zeolite led to an increase in the *p*XL yield from 75% to 97% at 523 K and 6.2 kPa of ethylene in the batch system.[33] Similarly, Zr-, Sn- and Ti-Beta zeo-

[a]*Max Planck Institute of Colloids and Interfaces, Department of Colloid Chemistry, 14476 Potsdam, Germany. E-mail: majd.al-naji@mpikg.mpg.de*
[b]*Laboratorio de Catálisis Heterogénea, Universidad Nacional de Colombia, 11001 Bogotá, Colombia*

†Electronic supplementary information (ESI) available. See DOI: 10.1039/d0gc01517b

lites with Lewis acid sites were found to be highly active and selective for the conversion of DMF to *p*XL in the presence of ethylene (6.2 MPa) at 523 K.[31,34] Of these, Zr-Beta exhibited the highest catalytic performance (DMF conversion = 99% and *p*XL selectivity = 90%).[34] Also, heteropolyacids and sulfonic acids supported on SiO_2 showed a high DMF conversion (94%) and *p*XL selectivity (85%), here due to enhanced Brønsted acid sites at 523 K, 2.0 MPa and 6 h of reaction time.[35,36] From the above investigations, high acid site density combined with high surface area seems to be essential for catalysts used in the Diels–Alder cycloaddition of DMF/ethylene followed by dehydration of the intermediate product. Alternatively, several trials were made for the synthesis of aromatics by Diels–Alder cycloaddition using furans and ethanol (as *in situ* ethylene source) over zeolite as catalysts in a batch system.[36–39] However, this approach requires high reaction temperatures to dehydrate ethanol to ethylene and leads to high amounts of by-products. An alternative route for the sustainable production of aromatics from furanics was proposed by replacing ethylene with different dienophiles such as acrylic acid (AA) or maleic anhydride (MA).[26,40–42] In this green and safe route, the reaction can be performed in the liquid phase at lower reaction temperatures (423 K–473 K) and without external gas pressure. Furthermore, competing reactions that lead to the wide range of by-products are suppressed, and the selectivity towards the targeted aromatics is increased. However, the synthesis of *p*XL utilizing this route was rarely described, as it comes with an additional elimination step of the intermidates to improve the *p*XL yield. However, this additional step can be avoided by performing this *in situ* cascade reactions in continous flow system. As a move in this direction, the two step batch synthesis of *p*XL from DMF and AA catalyzed by scandium(III) triflate ($Sc(OTf)_3$) in ionic liquids under mild reaction conditions was reported.[43] It was found that 48% of *p*XL and 22% of 2,5-dimethylbenzoic acid (DMBA) are formed in the 1st step. The consecutive 2nd step includes the decarboxylation of the *p*XL and DMBA mixture which improves the yield of *p*XL to 57%.[43] Similarly, the reaction between DMF and AA at room temperature was performed by using acidic ionic liquid ([Bmim]H_2SO_4) in a batch system.[28] After the 1st step at room temperature, a *p*XL yield of 45 mol% was achieved. A decarboxylation step at 473 K was again added to improve the yield of *p*XL.[28] From these multistep and homogenously-catalyzed *p*XL syntheses from DMF, we will move here to a more sustainable, heterogeneously catalyzed, continuous valorization of bio-based derivable DMF and AA to *p*XL and DMBA in the liquid phase (Scheme 1). The *in situ* triplet reaction includes Diels–Alder cycloaddition, dehydration and decarboxylation over different zeolites, *i.e.* Beta, ZSM-5 and Y, in a continuous flow-process under comparably mild reaction conditions at very high conversion and yields with a contact time of only 10.1 minutes (Scheme 1). We expect this integrated intrinsically benign and sustainable process to be of significant industrial potential for the production of *p*XL (Bp = 411.3 K) and DMBA (Bp = 559 K) from directly accessible products from biomass, as it might even reduce *p*XL costs due to the use of the flow system and simple separation of the products *via* a simple distillation step.

Results and discussion

Catalyst characterization

The different utilized zeolites were abbreviated as follows: zeolite framework (ZSM-5, Beta or Y), followed by (Si/Al molar ratio), *e.g.*, Beta(12.5). Prior to the catalytic experiments, all utilized H-form zeolites, *i.e.* ZSM-5(280), Beta(12.5, 90 and 150) and Y(80), were thoroughly characterized using N_2-sorption, X-ray diffraction (XRD), elemental analysis *via* inductively coupled plasma optical emission spectroscopy (ICP-OES) and temperature-programmed desorption of ammonia (NH_3-TPD). The experimental procedures of these characterization techniques are reported in the ESI.† The textural properties of the utilized zeolites are presented in Table 1. All catalysts were coded as follows: zeolite framework (Si/Al molar ratio).

The zeolites, *i.e.* ZSM-5(280), Y(80) and Beta(12.5, 90 and 150), showed standard adsorption–desorption isotherms, as well as the typical XRD patterns and no remarkable or unusual characteristics were observed, *cf.* Fig. S2–S4 in the ESI.† The total specific surface area of all catalysts was found to be in a range between 350 and 1250 $m^2\ g^{-1}$ corresponding mainly to the microporosity of the zeolites, showing the highest values for Y(80) and Beta(150), *i.e.* >1200 $m^2\ g^{-1}$, owing to their porous architecture. The lowest values are found for ZMS-5 (280) with 608 $m^2\ g^{-1}$. In addition to the specific microporous surface area, Hi-Beta(150) is an exception which showed a high

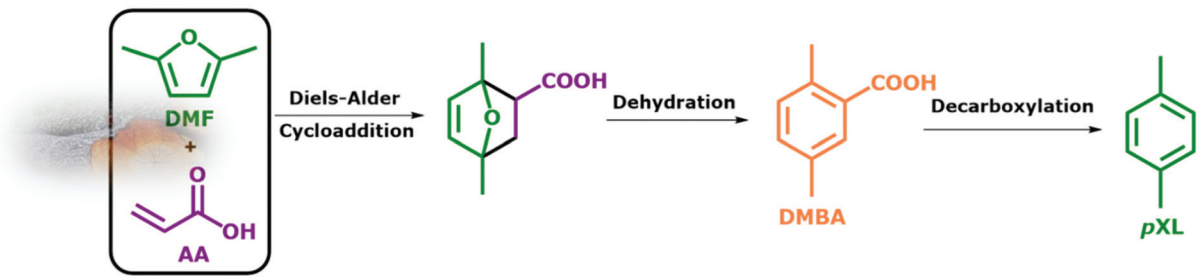

Scheme 1 The proposed three-in-one continuous reaction of DMF and AA to *p*XL and DMBA using zeolite as a catalyst.

Table 1 Textural properties deduced from N_2-sorption (NLDFT model of adsorption branch) and NH_3-TPD for different zeolites, *i.e.* ZSM-5(280), Y(80), Beta(12.5) and Beta(150), as well as hierarchical Beta(150), dealuminated Beta(150) and Na-ion exchange Beta(150)

Catalyst	V_{micro}/cm^3 g^{-1}	V_{total}/cm^3 g^{-1}	S_{micro}/m^2 g^{-1}	S_{total}/m^2 g^{-1}	Acid site density/μmol g^{-1}
ZSM-5(280)	0.11	0.20	511	608	51
Y(80)	0.26	0.46	1133	1276	162
Beta(150)	0.26	0.38	1180	1278	48
Beta(12.5)	0.16	0.40	724	835	285
Beta(90)	0.20	0.39	1078	1160	120
DeAl-Beta(150)	0.20	0.32	867	962	28
Na-Beta(150)	0.19	0.29	829	908	29
Hi-Beta(150)	0.07	0.45	137	357	39
Spent Beta(150)	0.20	0.29	840	925	36
Beta(150)_after 1st regeneration	0.23	0.35	1006	1186	44
Beta(150)_after 2nd regeneration	0.20	0.33	989	1217	49

specific mesoporous surface area (592 m^2 g^{-1}) as a result of successful alkaline treatment of Beta(150) to generate an additional mesoporous structure.[44–46]

Reaction of DMF with AA to synthesize *p*XL on different zeolite frameworks

Based on the available studies on the synthesis of *p*XL from DMF and ethylene, zeolites with a high Si/Al ratio are favored in the dehydration reaction due to their high catalytic performance.[47,48] In addition, it is well-known that improving zeolite hydrophobicity resulted in a thermodynamically favored water removal.[48] Therefore, we analyzed the performance of three different H-form zeolite frameworks, namely ZSM-5(280), Beta(150) and Y(80), in the conversion of DMF to *p*XL using AA (Fig. 1). In the absence of zeolite, no significant DMF conversion as well as no *p*XL was detected (Fig. 1), *i.e.* the presence of zeolite as an acid catalyst is crucial for the dehydration of the intermediate to DMBA, followed by decarboxylation of DMBA to *p*XL. Among the tested catalysts, Beta(150) and Y(80) showed complete conversion of DMF at 473 K after 10.1 min residence time (τ), while ZSM-5(280) showed a poor performance (36% of DMF conversion), *cf.* Fig. 1. Additionally, Beta(150) and Y(80) showed AA conversion of ~52%, whereas low AA conversion (25%) was found over ZSM-5(280), *cf.* Fig. S5 of the ESI.† Furthermore, *p*XL was found to be the main product, combined with the formation of DMBA as a by-product; Beta(150) exhibited the highest yield of *p*XL (83%) and DMBA (17%), and no further products could be identified. This *p*XL yield is the highest to be reported for DMF conversion with AA in comparison with 45% using [Bmim]HSO_4 and 57% in two steps in the presence of Sc(OTf)$_3$ and H_3PO_4.[28,43] ZSM-5(280) and Y(80) gave *p*XL in yields of 31.5% and 66.9% and DMBA in yields of 1.2% and 32.3%, respectively. The high *p*XL yield (83%) using Beta(150) is attributed to the 12-membered-ring and three-dimensional porous structure with diameters (6.6 × 6.7 Å) slightly larger than the *p*XL cross section diameter (6.3 Å) and smaller than *ortho* (*o*)- and *meta* (*m*)-xylenes (~6.8 Å), with no excess space (*e.g.* supercage) causing side reactions. Additionally, the Beta(150) structure selectively catalyzes the dehydration of the cycloadduct to *p*XL, *i.e.* small amounts of side reactions occur on it, as confirmed by TGA (Fig. 2), rendering it resistant to de-

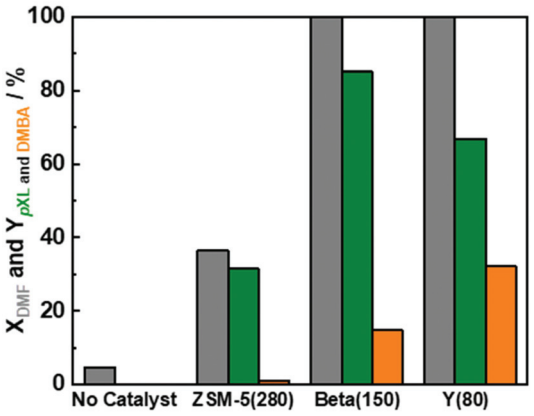

Fig. 1 DMF conversion (X_{DMF}) and *p*XL and DMBA yields (Y_{pXL} and Y_{DMBA}) after 2 h of time on stream in the absence of the catalyst and in the presence of three different zeolite frameworks, *i.e.* ZSM-5(280), Beta (150) and Y(80); reaction conditions: c_{DMF} = 0.3 M, c_{AA} = 0.7 M, T = 473 K, m_{cat} = 2 g, Q_{educt} = 0.3 cm^3 min^{-1}, $V_{reactor}$ = 3.04 cm^3, p_{system} = 3 MPa and τ = 10.1 min.

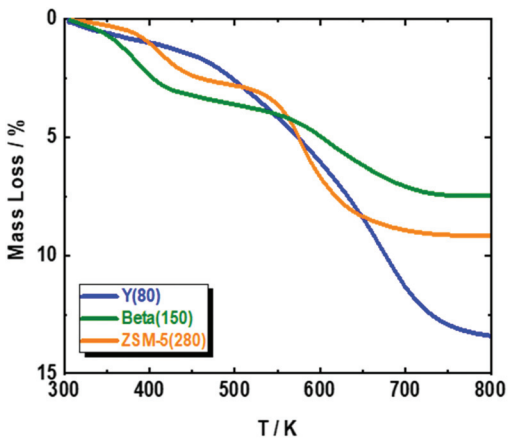

Fig. 2 TGA of spent ZSM-5(280), Beta(150) and Y(80) in the conversion of DMF and AA to *p*XL; reaction conditions: c_{DMF} = 0.3 M, c_{AA} = 0.7 M, T = 473 K, m_{cat} = 2 g, Q_{educt} = 0.3 cm^3 min^{-1}, $V_{reactor}$ = 3.04 cm^3, p_{system} = 3 MPa and τ = 10.1 min.

activation. This high catalytic performance of Beta zeolite with respect to other zeolites, *i.e.* ZSM-5(280) and Y(80), is in a good agreement with the previously reported studies on *p*XL synthesis from DMF.[26,30,31,42] The low selectivity of Y(80) is attributed to the larger pore diameter (7.3 × 7.3 Å) which allows the formation of higher amounts of by-products with higher molecular weights (coking), as confirmed by TGA for spent Y(80) and ZSM-5(280), *cf.* Fig. 2. Finally, ZSM-5(280) represented the lowest performance due to its smaller pore size (5.1 × 5.5 Å) in comparison to Beta and Y zeolites. In addition, ZSM-5(280) and Y(80) suffer from a rapid deactivation after 5 hours of time on stream (TOS) due to the deposition of higher amounts of coke in comparison to Beta(150), as confirmed by TGA (Fig. 2). The formation mechanism of the deposited coke is proposed in Scheme S1.† It depends on the pore size of the zeolite framework,[31,49] for instance when Y(280) was used, dimers and oligomers were observed on its surface, while ZSM-5(80) caused only the ring-opening of DMF, and alkylated aromatic and decarboxylated by-products, *cf.* ESI Scheme S1.†

Based on these results, Beta(150) was selected for further investigation on the influence of acid site density (using three different Si/Al molar ratios) and introduction of additional mesopores into the Beta zeolite framework. All tested Beta zeolites (12.5, 90 and 150) showed complete conversion of DMF (Fig. 3). Additionally, AA conversion was found to be between 50–60% for Beta zeolites with Si/AL molar ratios of 12.5, 90 and 150, respectively (Fig. S6 at ESI†). Beta(12.5) exhibited the lowest yield of *p*XL (40%) which could speculatively be attributed to its high density of acid sites that can stimulate other side reactions, *e.g.* cracking of *n*-heptane and ring-opening of DMF, leading to the formation of other side products. Moreover, it is well-known that the dehydration reaction is thermodynamically favored by increasing the hydrophobicity of the zeolite by using high Si/Al molar ratios.[48] This improvement in the catalytic performance in comparison with Beta (12.5) can be clearly seen when using Beta(90) and Beta(150), which showed higher yield of *p*XL (77% and 80%), *cf.* Fig. 3.

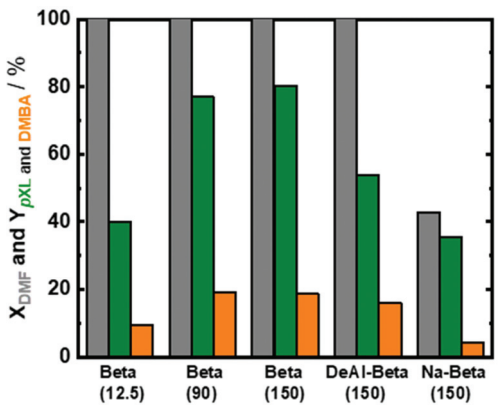

Fig. 3 DMF conversion (X_{DMF}) and *p*XL and DMBA yields (Y_{pXL} and Y_{DMBA}) after 2 h of time on stream over Beta zeolite with different Si/Al molar ratios (25, 90 and 150), as well as DeAl-Beta(150) and Na-Beta (150); reaction conditions: c_{DMF} = 0.3 M, c_{AA} = 0.7 M, T = 473 K, m_{cat} = 2 g, Q_{educt} = 0.3 cm^3 min^{-1}, $V_{reactor}$ = 3.04 cm^3, p_{system} = 3 MPa, and τ = 10.1 min.

In an attempt to improve the *p*XL yield, introduction of mesopores to the micropores in Beta(150) *via* alkaline treatment was performed, *cf.* the ESI† for the details on mesopore introduction. Hierarchical Beta(150) is coded as follows: Hi-Beta(150). The alkaline treatment was successful and Hi-Beta (150) showed, in addition to the presence of micropores, a high specific mesoporous surface area (294 m^2 g^{-1}) in comparison to Beta(150) which possesses a very low specific mesoporous surface area (Table 1 and Fig. S2 in the ESI†). Additionally, TEM images of Beta(150) and Hi-Beta(150) show a clear change in the morphology of Beta(150) after alkaline treatment, *cf.* ESI, Fig. S7.† The performance of Hi-Beta(150) in the conversion of DMF and AA to *p*XL was compared with Beta (150), *viz.* ESI Fig. S8.† Under the tested reaction conditions, DMF conversion completed, and no improvement in *p*XL and DMBA yields was observed by the introduction of mesopores to Beta(150) even after 5 h of time on stream (TOS), *cf.* ESI Fig. S8.† This suggests that under these reaction conditions the conversion of DMF with AA to *p*XL is free of diffusion limitations and additional mesopores do not have a positive impact on the *p*XL yield, which is in line with the previous study.[30,32]

In an attempt to improve the catalytic performance of Beta (150), it was subjected to two different treatments, *i.e.*, the dealumination process and ion-exchange of Beta(150) with Na, respectively. Throughout the manuscript, the dealuminated Beta(150) and Na-ion exchanged Beta(150) are coded as follows: DeAl-Beta(150) and Na-Beta(150), respectively. The details of these treatments and experimental procedure are described in the ESI.† Furthermore, the textural properties of these synthesized DeAl-Beta(150) and Na-Beta(150) are reported in Table 1. Complete DMF conversion was achieved over DeAl-Beta(150), while the *p*XL yield reduced to 54% in comparison with non-treated Beta(150). In contrast, low AA conversion (<50%) was observed over the treated Beta(150), *viz.* Fig. S6 in the ESI.† This indicates that DeAl-Beta(150) facilitates the occurrence of side reactions that led to coke deposition on the catalyst. Whereas, Na-Beta(150) showed a significant decrease in DMF conversion from 100% to 42% with respect to the non-treated Beta(150), *cf.* Fig. 3. Also, the *p*XL yield dropped from 80% to 35% with Na-Beta(150), and the DMBA yield was reduced from 18% to 4% in the presence of Na-Beta(150), *cf.* Fig. 3. These results are attributed to the drop in the specific surface area and total density of acid sites (confirmed by N_2-sorption and NH_3-TPD) caused by the treatment of Beta(150) *via* Na-ion exchange (Table 1). Based on these results, Beta(150) was selected for further optimization of the reaction conditions. Moreover, the stability of Beta(150) under the optimum reaction conditions was evaluated. Finally, the performance of Beta(150) in the flow process and batch experiment was assessed.

Therefore, reaction temperature, residence time, DMF/AA molar ratio were adjusted using Beta(150) to maximize the formation of *p*XL from DMF. In addition to the reaction temperature mentioned above (473 K), two additional reaction temp-

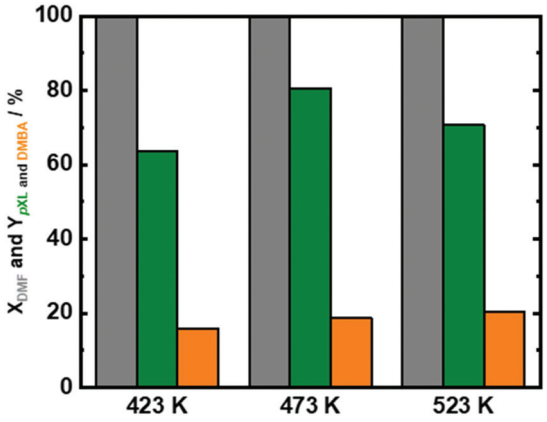

Fig. 4 DMF conversion (X_{DMF}) and *p*XL and DMBA yields (Y_{pXL} and Y_{DMBA}) after 2 h of time on stream as a function of reaction temperature (423 K, 473 K and 523 K); reaction conditions: c_{DMF} = 0.3 M, c_{AA} = 0.7 M, m_{cat} = 2 g, Q_{educt} = 0.3 cm^3 min^{-1}, $V_{reactor}$ = 3.04 cm^3, p_{system} = 3 MPa and τ = 10.1 min.

eratures were tested (423 K and 523 K). Over the whole analyzed temperature range, DMF was completely converted (Fig. 4), and the AA conversion was found to be ~50% (Fig. S9 in the ESI†). As expected, at a low reaction temperature (423 K), a lower *p*XL yield (64%) was found, *cf.* Fig. 4. Unexpectedly, a drop in the *p*XL yield was also observed at a high reaction temperature (523 K). This point is correlated to the occurrence of side reactions for the reactants (DMF or AA), as well as reactions between products (*p*XL and DMBA) at such high temperatures (Scheme S1 in the ESI†). Noteworthily, no significant differences in the DMBA yield (15–19%) were observed over all tested reaction temperatures.

Based on the abovementioned results, a temperature of 473 K was selected, and the influence of residence time (τ) under these reaction conditions was investigated (Fig. 5). In addition to 10.1 min as the residence time, additional experiments with 3.04 min, 5.0 min and 30.4 min residence times were performed. At all utilized residence times, above 96% conversion of DMF combined with ~50% AA conversion was recorded (Fig. 5 and Fig. S10 at ESI†). Furthermore, *p*XL and DMBA were the only products that were identified under these reaction conditions. Increasing the residence time from 3.04 min to 5.01 min and further to 10.1 min (Fig. 5), led to improved *p*XL yields from 59.3% to 70% and 80%, respectively. In contrast, the increase of residence time (t) from 3.04 min to 5.01 min to 10.1 min and 30.4 min is associated with the drop in the DMBA yield from 31.7% to 16% to 14% and 13%, respectively. The low *p*XL yield (59.3%) at a residence time of 3.01 min is due to shorter contact time between the substrate and Beta(150) which led to inefficient dehydration/decarboxylation of the cycloaddition product (Fig. 5). A further increase in residence time from 10.1 min to 30.4 min showed no significant change in the *p*XL yield (~83%), as well as DMBA yields of ~13%, *cf.* Fig. 5. These results further indicate that the formation of *p*XL is mainly through DMBA decarboxylation.

Taking into consideration the minor differences in the catalyst performance in 10.1 min and 30.4 min and the 3 times higher space–time yield of *p*XL after 10.1 min, 10.1 min was selected to assess the influence of DMF/AA molar ratio variation. DMF conversion was completed at all utilized DMF/AA molar ratios (Fig. 6), *i.e.* 0.14, 0.27, 0.45, 1.0 and 1.1. Additionally, AA conversion was linearly increased from 23% to 80% with increasing DMF/AA molar ratio from 0.14 to 1 (Fig. 6). In contrast, the *p*XL yield was found to be slightly increased (from 77% to 80%) using DMF/AA molar ratios between 0.14, 0.27 and 0.45 (Fig. 6). Equimolar DMF and AA led to a decrease in the *p*XL yield from 80% to 61% (Fig. 6). A further reduction of the AA amount (DMF/AA molar ratio =

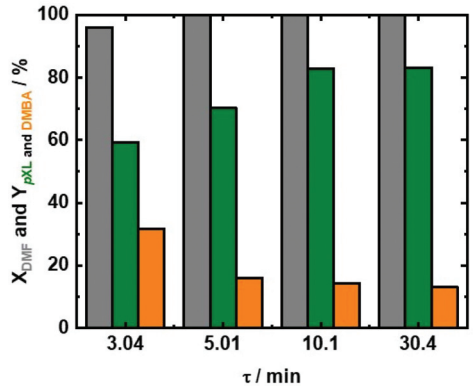

Fig. 5 DMF conversion (X_{DMF}) and *p*XL and DMBA yields (Y_{pXL} and Y_{DMBA}) after 2 hours of time on stream as a function of residence time (τ); reaction conditions: c_{DMF} = 0.3 M, c_{AA} = 0.7 M, T = 473 K, m_{cat} = 2 g, Q_{educt} = 0.6 cm^3 min^{-1}, 0.3 cm^3 min^{-1} and 0.1 cm^3 min^{-1}, $V_{reactor}$ = 3.04 cm^3, p_{system} = 3 MPa and τ = 5.0 min, 10.1 min and 30.4 min.

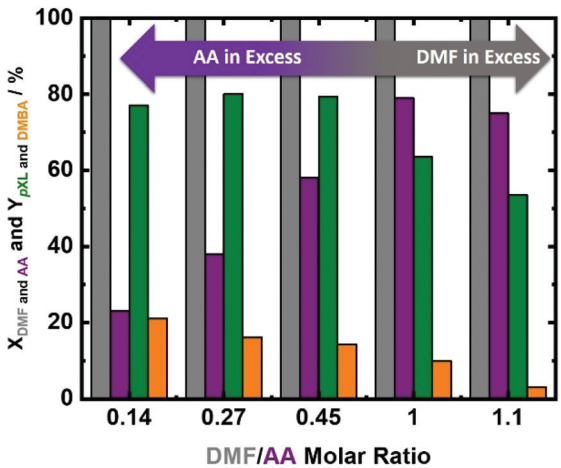

Fig. 6 DMF and AA conversion ($X_{DMF\ and\ AA}$) and *p*XL and DMBA yields (Y_{pXL} and Y_{DMBA}) after 2 h of time on stream as a function of DMF/AA molar ratio (0.14, 0.27, 0.45, 1.0 and 1.1); reaction conditions: c_{DMF} = 0.09 M, 0.18 M, 0.30 M, 0.70 M and 0.76 M, c_{AA} = 0.70 M, T = 473 K, m_{cat} = 2 g, Q_{educt} = 0.3 cm^3 min^{-1}, $V_{reactor}$ = 3.04 cm^3, p_{system} = 3 MPa and τ = 10.1 min.

1.1), caused further decrease of *p*XL yield to 52% (Fig. 6). This behavior can be explained by the kinetics of bimolecular reactions (for the cycloaddition) which appears to be fast with an excess of AA. In addition, too high amounts of DMF lead to undesired side reactions, such as dimerization and oligomerisation of DMF, as well as DMF hydrolysis to 2,5-hexandione (proposed in Scheme S1†), which obviously lowers the yield of *p*XL. Finally, this observation suggests that the presence of an excess of AA is required to obtain a high *p*XL yield and selectivity (Fig. 6).

Using Beta(150) under the optimum reaction conditions, *i.e.*, c_{DMF} = 0.3 M, c_{AA} = 0.7 M, T = 473 K, m_{cat} = 2 g, Q_{educt} = 0.3 cm^3 min^{-1}, $V_{reactor}$ = 3.04 cm^3, p_{system} = 3 MPa, and τ = 10.1 min, the turnover frequency (TOF) was calculated by considering the total acid site density of Beta(150). The calculated TOF was 48 h^{-1} with a *p*XL space–time yield (STY_{pXL}) of 0.23 kg_{pXL} h^{-1} kg_{cat}^{-1}. The calculated TOF (48 h^{-1}) for Beta (150) in this reaction system (DMF and AA in a continuous flow system) was lower than the reported TOF values for Zr-Beta (121 h^{-1}), Al-Beta (122 h^{-1}), Sn-Beta (113 h^{-1}) and Ti-Beta (65 h^{-1}) for the conversion of DMF with ethylene in a batch system at 523 K.[31] The low TOF value for Beta(150) in comparison to the reported TOF values for Zr-Beta, Al-Beta, Sn-Beta and Ti-Beta is due to a low operational temperature (473 K) of our system, as well as the different reaction mechanisms (the occurrence of an additional decarboxylation step of DMBA).

Catalyst stability

Under the optimized reaction conditions, the performance of fresh Beta150 under 10 hours of time on stream (TOS) was evaluated (Fig. 7). It can be seen that Beta(150) showed a stable performance with complete DMF conversion and *p*XL yield of ~80%, after 10 hours of TOS (Fig. 7). In addition, AA conversion remained stable after 10 h of TOS (Fig. S11 at ESI†). However, a slight drop in the *p*XL yield after 8 hours of TOS was observed in parallel with a reduction in the specific surface area from 1278 m^2 g^{-1} to 925 m^2 g^{-1} and acid site density from 48 μmol g^{-1} to 36 μmol g^{-1} (Table 1 and Fig. S12 at ESI†). With the changes of the textural properties, we find the deposition of (~20%) of carbonaceous species after 10 h of TOS, which is confirmed by TGA (Fig. S14 at ESI†). The implementation of regeneration cycles *via* thermal treatment of the used Beta(150) have been proposed as a strategy to extend the long-term use of the catalysts (the details of the regeneration procedure is described in the ESI†). Applying the regeneration steps resulted in successful recovery of the catalyst performance back to the level of the freshly used catalyst (Fig. 7). Characterization after each regeneration step revealed that the textural properties and crystalline structure were mostly restored (Table 1 and Fig. S12 in the ESI†). Of course, practical catalyst reactivation processes in flow reactors preferentially occur in the switched flow mode, *e.g.* under different solvents. We assume that the side products under optimized conditions are DMF oligomers only, which are insoluble in the used solvent (*n*-heptane).

Catalytic performance in flow and batch reactors

It is clear that a contact time of 10.1 min for full conversion in the continuous flow process is very short when compared to previous reports on those using the batch system, and we attribute this to the perfect heat transfer and reaction profile in flow reactors. To underline this point, the catalytic performance was analyzed in two types of reactors, *i.e.* the continuous flow system *vs.* batch system. We exposed the same amount of Beta(150) to catalytic experiments for 8 h in both systems (Fig. 8). As reported above Beta(150) in a continuous flow system showed quantitative conversion of DMF with a *p*XL yield of 80% and a DMBA yield of 10%. Moreover, Beta(150) in a continuous flow system showed higher AA conversion (~60%) than that in the batch system (40%), *viz.* Fig. S14 in the ESI.† The batch experiment using Beta(150) revealed a low DMF conversion (40%) and

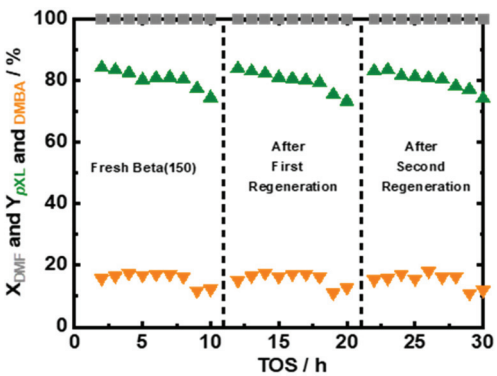

Fig. 7 DMF conversion (X_{DMF}) and *p*XL and DMBA yields (Y_{pXL} and Y_{DMBA}) as a function of time on stream (TOS) for fresh Beta(150) after two regeneration steps; reaction conditions: c_{DMF} = 0.3 M, c_{AA} = 0.7 M, m_{cat} = 2 g, Q_{educt} = 0.3 cm^3 min^{-1}, $V_{reactor}$ = 3.04 cm^3, p_{system} = 3 MPa, and τ = 10.1 min.

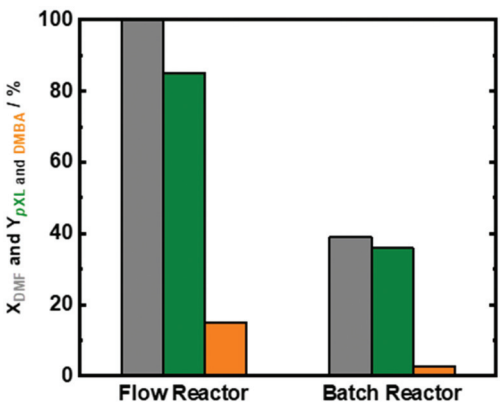

Fig. 8 DMF conversion (X_{DMF}) and *p*XL and DMBA yields ($Y_{pXL\ and\ DMBA}$) over Beta(150) after 8 hours in a continuous flow system and batch reactor; reaction conditions in the continuous flow system: c_{DMF} = 0.3 M, c_{AA} = 0.7 M, T = 473 K, m_{cat} = 2 g, Q_{educt} = 0.3 cm^3 min^{-1}, $V_{reactor}$ = 3.04 cm^3, p_{system} = 3 MPa, and t = 10.1 min; reaction conditions in the batch reactor: c_{DMF} = 0.3 M, c_{AA} = 0.7 M, T = 473 K, m_{cat} = 2 g, n = 400 rpm, p = 3 MPa of N_2.

*p*XL and DMBA yield of 34% and 4%, respectively. The low DMF conversion and low *p*XL and DMBA yields in the batch system are attributed to rapid catalyst deactivation because the products are not flushed out, but remain on the catalyst. The flow system offers a short contact time (10.1 min) as well as a fresh supply of the reaction solution, which allows a longer operation time without deactivation. Furthermore, TGA characterization of the spent Beta(150) in the batch reactor showed 47 wt% coke or deposits while the experiment conducted in a continuous flow reactor showed a weight loss of 10 wt% (Fig. S14 in the ESI†). These experiments clearly support the view that the flow system is favored to run the present system economically and in a sustainable fashion.[12,50]

Conclusions

In summary, a three-in-one reaction, Diels–Alder cycloaddition of 2,5-dimethylfuran to acrylic acid, dehydration to form the phenyl-ring, and final decarboxylation to *p*-xylene, was successfully performed in a continuous flow system over Beta zeolite, using *n*-heptane as a solvent. This reaction requires a catalyst with specific parameters to obtain the optimum performance. We found that the combination of high specific surface area (mainly microporous) with a 3D pore architecture of 6.6 × 6.7 Å size, and a medium to high acid site density in the range of 50 μmol g^{-1} in a zeolite promote the two follow up reactions, while alternative self-condensation reactions are suppressed. Furthermore, an optimal balance between the 2,5-dimethylfuran and acrylic acid molar ratios is likely important for efficient *p*-xylene production. As a result of this process, a highly valuable product mixture consisting of *p*-xylene and 2,5-dimethylbenzoic acid is obtained which can be simply separated based on their boiling points. This benign process provides an alternative and efficient pathway to produce *p*-xylene from renewable resources, *e.g.* lignocellulosic biomass, which could substitute its production pathway from fossil oils within the biorefinery scheme. To apply this process on a large scale, a detailed microkinetics study of this reaction is greatly required, which will provide more insight into the underlying mechanism. Finally, the evaluation of the final cost of the products through detailed techno-economic studies will reveal the industrial relevance of the proposed strategy.

Experimental section

Different types of zeolites (Beta, ZSM-5 and Y) in H-form were supplied by Clariant and Zeolyst. The material details that have been used in this work are described in the ESI.† All utilized catalysts were thoroughly characterized *via* N_2-sorption, XRD, NH_3-TPD and TGA. The experimental details and procedures of the characterization techniques are also described in the ESI.†

The reaction of 2,5-dimethylfuran (DMF) in the presence of acrylic acid (AA) was studied in a homemade continuous-flow fixed bed reactor similar to the one described in our previous studies (Fig. S1A in the ESI†).[12,17] In a typical experiment, a solution of DMF (0.3 M) with acrylic acid (0.7 M) in *n*-heptane was fed using a HPLC pump through a stainless steel tubing. A heating unit consisting of a pre-heated tube, tubular reactor and thermocouple was placed in a homemade aluminum heating mantle (Fig. S1B at ESI†). A stainless steel tubular reactor from Swagelok with an inner diameter (ID) = 4.6 mm and length (l) = 25 cm was used to perform the catalytic experiments. Prior to sampling, internal liquid pressure was set at 3.0–3.5 MPa using a back-pressure regulator. For qualitative and quantitative analyses, a sample of *ca.* 2.0 cm^3 was collected and analyzed *via* gas chromatography (GC-MS) and high performance liquid chromatography (HPLC). More details about the experimental setup, procedures and reactants and product analysis can be found in the ESI.†

Conflicts of interest

There are no conflicts to declare.

Acknowledgements

The authors are grateful for the financial support from the Max Planck Society. Jose Alirio Mendoza Mesa thanks the "Gobernación del Tolima" and Colfuturo for a research scholarship granted through Convocatoria 727-2017 of Colciencias. Thanks are also extended to Jessica Brandt, Rona Pitschke and Antje Völkel of the Max Planck Institute of Colloids and Interfaces for elemental analysis, TEM and TGA measurements, respectively. The effort of the electrical and mechanical workshops at the Max Planck Institute of Colloids and Interfaces is greatly acknowledged. Our special thanks goes to Valerio Cersani for the design and idea of the table of contents. Open Access funding provided by the Max Planck Society.

References

1 D. Esposito and M. Antonietti, *Chem. Soc. Rev.*, 2015, **44**, 5821–5835.
2 Y. Liao, S.-F. Koelewijn, G. Van den Bossche, J. Van Aelst, S. Van den Bosch, T. Renders, K. Navare, T. Nicolaï, K. Van Aelst, M. Maesen, H. Matsushima, J. M. Thevelein, K. Van Acker, B. Lagrain, D. Verboekend and B. F. Sels, *Science*, 2020, **367**, 1385–1390.
3 G. W. Huber, J. N. Chheda, C. J. Barrett and J. A. Dumesic, *Science*, 2005, **308**, 1446–1450.
4 Y. Roman-Leshkov, C. J. Barrett, Z. Y. Liu and J. A. Dumesic, *Nature*, 2007, **447**, 982–985.
5 C. K. W. Arthur, J. Ragauskas, B. H. Davison, G. Britovsek, J. Cairney, C. A. Eckert, W. J. Frederick Jr., J. P. Hallett, D. J. Leak, C. L. Liotta, J. R. Mielenz, R. Murphy, R. Templer and T. Tschaplinski, *Science*, 2006, **311**, 484–489.

6 D. A. S. Edward, L. Kunkes, R. M. West, J. C. Serrano-Ruiz, C. A. Gärtner and J. A. Dumesic, *Science*, 2008, **322**, 417–421.
7 *Zeolites and Zeolite-like Materials*, ed. W. S. T. Ennaert, J. Dijkmans, M. Dusselier and B. F. Sels, Elsevier, Amesterdam, 2016.
8 J. C. Serrano-Ruiz and J. A. Dumesic, *Energy Environ. Sci.*, 2011, **4**, 83–99.
9 P. C. Bruijnincx and B. M. Weckhuysen, *Angew. Chem., Int. Ed.*, 2013, **52**, 11980–11987.
10 D. M. Alonso, S. G. Wettstein and J. A. Dumesic, *Chem. Soc. Rev.*, 2012, **41**, 8075–8098.
11 B. Kumru, J. Mendoza Mesa, M. Antonietti and M. Al-Naji, *ACS Sustainable Chem. Eng.*, 2019, **7**, 17574–17579.
12 F. Brandi, M. Bäumel, V. Molinari, I. Shekova, I. Lauermann, T. Heil, M. Antonietti and M. Al-Naji, *Green Chem.*, 2020, **22**, 2755–2766.
13 D. Zhao, D. Rodriguez-Padron, K. S. Triantafyllidis, Y. Wang, R. Luque and C. Len, *ACS Sustainable Chem. Eng.*, 2020, **8**, 3091–3102.
14 S. Mhadmhan, A. Franco, A. Pineda, P. Reubroycharoen and R. Luque, *ACS Sustainable Chem. Eng.*, 2019, **7**, 14210–14216.
15 M. Braun and M. Antonietti, *Green Chem.*, 2017, **19**, 3813–3819.
16 M. Al-Naji, M. Popova, Z. Chen, N. Wilde and R. Gläser, *ACS Sustainable Chem. Eng.*, 2019, **8**, 393–402.
17 M. Al-Naji, B. Puertolas, B. Kumru, D. Cruz, M. Baumel, B. Schmidt, N. V. Tarakina and J. Perez-Ramirez, *ChemSusChem*, 2019, **12**, 2628–2636.
18 M. Al-Naji, J. Van Aelst, Y. Liao, M. d'Hullian, Z. Tian, C. Wang, R. Gläser and B. F. Sels, *Green Chem.*, 2020, **22**, 1171–1181.
19 M. Al-Naji, A. Yepez, A. M. Balu, A. A. Romero, Z. Chen, N. Wilde, H. Li, K. Shih, R. Gläser and R. Luqueb, *J. Mol. Catal. A: Chem.*, 2016, **417**, 145–152.
20 H. Xiao, B. Hou, P. Zeng, A. Jiang, X. Hou and J. Liu, *Fuel*, 2017, **192**, 53–59.
21 M. Wei, S. Li, J. Liu, G. Guo, Z. Sun and H. Xiao, *Fuel*, 2017, **192**, 208–217.
22 R. A. Sheldon, *Green Chem.*, 2014, **16**, 950–963.
23 A. Maneffa, P. Priecel and J. A. Lopez-Sanchez, *ChemSusChem*, 2016, **9**, 2736–2748.
24 V. J. Margarit, E. M. Gallego, C. Paris, M. Boronat, M. Moliner and A. Corma, *Green Chem.*, 2020, **22**, 5123–5131.
25 K. Smith, M. Pampel and P. Feng, *IHS Chemical Chemical Economics Handbook–Xylenes*, 2015.
26 A. E. Settle, L. Berstis, N. A. Rorrer, Y. Roman-Leshkóv, G. T. Beckham, R. M. Richards and D. R. Vardon, *Green Chem.*, 2017, **19**, 3468–3492.
27 Z. Lin, M. Ierapetritou and V. Nikolakis, *AIChE J.*, 2013, **59**, 2079–2087.
28 L. Ni, J. Xin, K. Jiang, L. Chen, D. Yan, X. Lu and S. Zhang, *ACS Sustainable Chem. Eng.*, 2018, **6**, 2541–2551.
29 Y. T. Cheng, Z. Wang, C. J. Gilbert, W. Fan and G. W. Huber, *Angew. Chem., Int. Ed.*, 2012, **51**, 11097–11100.
30 C. L. Williams, C.-C. Chang, P. Do, N. Nikbin, S. Caratzoulas, D. G. Vlachos, R. F. Lobo, W. Fan and P. J. Dauenhauer, *ACS Catal.*, 2012, **2**, 935–939.
31 C.-C. Chang, H. Je Cho, J. Yu, R. J. Gorte, J. Gulbinski, P. Dauenhauer and W. Fan, *Green Chem.*, 2016, **18**, 1368–1376.
32 C.-C. Chang, S. K. Green, C. L. Williams, P. J. Dauenhauer and W. Fan, *Green Chem.*, 2014, **16**, 585–588.
33 H. J. Cho, L. Ren, V. Vattipalli, Y.-H. Yeh, N. Gould, B. Xu, R. J. Gorte, R. Lobo, P. J. Dauenhauer, M. Tsapatsis and W. Fan, *ChemCatChem*, 2017, **9**, 398–402.
34 J. Yu, S. Zhu, P. J. Dauenhauer, H. J. Cho, W. Fan and R. J. Gorte, *Catal. Sci. Technol.*, 2016, **6**, 5729–5736.
35 X. Feng, C. Shen, C. Tian and T. Tan, *Ind. Eng. Chem. Res.*, 2017, **56**, 5852–5859.
36 Y. P. Wijaya, H. P. Winoto, Y.-K. Park, D. J. Suh, H. Lee, J.-M. Ha and J. Jae, *Catal. Today*, 2017, **293–294**, 167–175.
37 I. F. Teixeira, B. T. Lo, P. Kostetskyy, M. Stamatakis, L. Ye, C. C. Tang, G. Mpourmpakis and S. C. Tsang, *Angew. Chem., Int. Ed.*, 2016, **55**, 13061–13066.
38 L. Ye, I. Teixeira, B. T. W. Lo, P. Zhao and S. C. Edman Tsang, *Chem. Commun.*, 2017, **53**, 9725–9728.
39 I. F. Teixeira, B. T. W. Lo, P. Kostetskyy, L. Ye, C. C. Tang, G. Mpourmpakis and S. C. E. Tsang, *ACS Catal.*, 2018, **8**, 1843–1850.
40 S. Thiyagarajan, H. C. Genuino, M. Sliwa, J. C. van der Waal, E. de Jong, J. van Haveren, B. M. Weckhuysen, P. C. Bruijnincx and D. S. van Es, *ChemSusChem*, 2015, **8**, 3052–3056.
41 S. Thiyagarajan, H. C. Genuino, J. C. van der Waal, E. de Jong, B. M. Weckhuysen, J. van Haveren, P. C. Bruijnincx and D. S. van Es, *Angew. Chem., Int. Ed.*, 2016, **55**, 1368–1371.
42 E. Mahmoud, J. Yu, R. J. Gorte and R. F. Lobo, *ACS Catal.*, 2015, **5**, 6946–6955.
43 L. Ni, J. Xin, H. Dong, X. Lu, X. Liu and S. Zhang, *ChemSusChem*, 2017, **10**, 2394–2401.
44 P. Y. Dapsens, C. Mondelli and J. Perez-Ramirez, *Chem. Soc. Rev.*, 2015, **44**, 7025–7043.
45 J. Van Aelst, D. Verboekend, A. Philippaerts, N. Nuttens, M. Kurttepeli, E. Gobechiya, M. Haouas, S. P. Sree, J. F. M. Denayer, J. A. Martens, C. E. A. Kirschhock, F. Taulelle, S. Bals, G. V. Baron, P. A. Jacobs and B. F. Sels, *Adv. Funct. Mater.*, 2015, **25**, 7130–7144.
46 D. Verboekend, N. Nuttens, R. Locus, J. Van Aelst, P. Verolme, J. C. Groen, J. Perez-Ramirez and B. F. Sels, *Chem. Soc. Rev.*, 2016, **45**, 3331–3352.
47 R. Otomo, T. Yokoi and T. Tatsumi, *Appl. Catal., A*, 2015, **505**, 28–35.
48 H. Kobayashi, H. Yokoyama, B. Feng and A. Fukuoka, *Green Chem.*, 2015, **17**, 2732–2735.
49 Y. Mathieu, A. Corma, M. Echard and M. Bories, *Appl. Catal., A*, 2014, **469**, 451–465.
50 R. Gerardy, D. P. Debecker, J. Estager, P. Luis and J. M. Monbaliu, *Chem. Rev.*, 2020, **120**(15), 7219–7347.